JACS
JOURNAL OF THE AMERICAN CHEMICAL SOCIETY

ARTICLE

pubs.acs.org/JACS

Probing the Structure of the Crystalline Core of Field-Aligned, Monodisperse, Cylindrical Polyisoprene-*block*-Polyferrocenylsilane Micelles in Solution Using Synchrotron Small- and Wide-Angle X-ray Scattering

Joe B. Gilroy,[†] Paul A. Rupar,[†] George R. Whittell,[†] Laurent Chabanne,[†] Nicholas J. Terrill,[‡] Mitchell A. Winnik,[*,§] Ian Manners,[*,†] and Robert M. Richardson[*,⊥]

[†]School of Chemistry, University of Bristol, Bristol, United Kingdom, BS8 1TS
[‡]Diamond Light Source Ltd, Diamond House, Harwell Science and Innovation Campus, Didcot, United Kingdom, OX11 0DE
[§]Department of Chemistry, University of Toronto, Toronto, Ontario, Canada, M5S 3H6
[⊥]H. H. Wills Physics Laboratory, University of Bristol, United Kingdom, BS8 1TL

S *Supporting Information*

ABSTRACT: The self-assembly of block copolymers in selective solvents represents a powerful approach to functional core–shell nanoparticles. Crystallization of the core can play a critical role in directing self-assembly toward desirable, nonspherical morphologies with low mean interfacial curvature. Moreover, epitaxial growth processes have been implicated in recent advances that permit access to monodisperse cylinders, cylindrical block comicelles with segmented cores and/or coronas, and complex hierarchical architectures. However, how the core-forming block crystallizes in an inherently curved nanoscopic environment has not been resolved. Herein we report the results of synchrotron small-angle X-ray scattering (SAXS) and wide-angle X-ray scattering (WAXS) studies of well-defined, monodisperse crystalline-coil polyisoprene-*block*-polyferrocenylsilane cylindrical micelles aligned in an electric field. WAXS studies of the aligned cylinders have provided key structural information on the nature of the PFS micelle core together with insight into the role of polymer crystallinity in the self-assembly of these and potentially related crystalline-coil block copolymers.

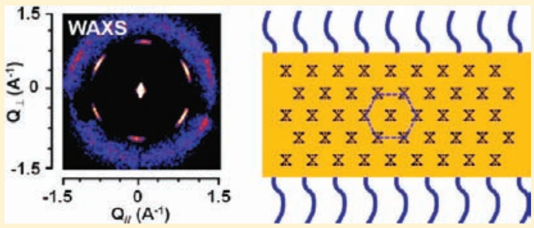

INTRODUCTION

Functional one-dimensional (1D) nanostructures have received considerable recent attention due to their emerging utility in a variety of materials-based applications.[1] Several strategies toward the realization of the nanomaterials exist, including the self-assembly of organic molecules[2] and nanoparticles,[3,4] functionalization of virus particles,[5] self-assembly of inorganic[6] and carbon-based materials,[7] synthesis of molecular brushes,[8] and self-assembly of "hairy-rod" macromolecules[9] and oligopeptides.[10] Recent advances concerning the solution self-assembly of block copolymers suggest a promising alternative strategy for the realization of functional 1D nanostructured materials.[11] A wide range of morphologies including disks,[12] helices,[13] toroids,[14] vesicles,[15] and more complex structures[16] have been reported. Cylindrical (or nanofiber) micelles[17−20] based on block copolymers have emerged as interesting examples due to their potential utility as templates for nanoparticles,[21] as precursors for nanostructured ceramic materials,[22] as strength-enhancing additives in plastics,[23] as etch resists,[24] and in drug delivery.[25] In addition, the structural control and the ability to "lock-in" structures by making them permanent through core and coronal cross-linking chemistries offer potential advantages for a range of applications.[26]

Most studies of the solution self-assembly of block copolymers have involved materials in which the core-forming block is amorphous. Recently, the solution self-assembly of crystalline-coil block copolymers has attracted growing attention with the demonstration that crystallization of the core can direct self-assembly toward morphologies with intrinsically low interfacial curvature, such as cylinders and platelets that are otherwise difficult to access.[17,20,27] The self-assembly of diblock copolymers containing a polyferrocenyldimethylsilane (PFS) metalloblock as the crystalline, core-forming segment has provided a route to monodisperse cylindrical micelles[29] as well as a variety of complex architectures including block comicelles,[30,31] hierarchical scarf-like micelles and micelle brushes,[32] and pointed ovals.[33] The control exhibited in these systems arises from a crystallization-driven living self-assembly growth mechanism, which is believed to operate via epitaxial growth of PFS at the micelle ends. Recent developments indicate that this process is extendable to crystallizable, core-forming blocks based on other polymer systems, including organic materials.[20,32,34] Understanding how the core-forming block crystallizes

Received: August 7, 2011
Published: September 01, 2011

in a nanoscopic environment with inherent curvature is therefore of key importance.

We previously reported preliminary studies of the liquid-crystalline properties of monodisperse 730 nm long PI_{550}-*b*-PFS_{50} cylindrical micelles that revealed an electric field-responsive nematic-like phase at a concentration of 50 mg mL^{-1} in decane.[29] In the present study, we examined a field-aligned sample of monodisperse PFS-*b*-polyisoprene (PI) cylindrical micelles grown from PFS-*b*-polydimethylsiloxane (PDMS) crystallites by synchrotron small-angle X-ray scattering (SAXS) and wide-angle X-ray scattering (WAXS). Crucially, the alignment behavior confirmed by SAXS studies allowed for the structure of the crystalline PFS micelle core to be studied and for the orientation of the PFS polymer chains with respect to the direction of cylinder growth to be explored. These results represent a significant advance toward understanding the mechanism of crystallization-driven living self-assembly in this and other systems.

RESULTS

The amphiphilic block copolymers employed in this study were prepared by the previously reported sequential living anionic polymerization of dimethylsila[1]ferrocenophane **1** and an appropriate co-monomer.[35] PFS_{28}-*b*-$PDMS_{560}$ **2**, where the subscripts refer to the number-average degree of polymerization, was prepared by addition of hexamethylcyclotrisiloxane [$(Me_2SiO)_3$] containing 12-crown-4 in THF to a solution of *n*-BuLi-initiated living PFS before the addition of trimethylsilylchloride (TMSCl) to quench the living chain. PI_{637}-*b*-PFS_{53} **3** was prepared by addition of **1** to a solution of *s*-BuLi-initiated PI, before the living chain was terminated by addition of a few drops of degassed methanol. The molecular weight of the diblock copolymers was determined using a combination of gel permeation chromatography (GPC) and integration data from ^{1}H NMR spectra. The polydispersity index (PDI) of the diblock copolymers was determined by GPC analysis (Table 1).

The monodisperse cylindrical micelles of PI_{637}-*b*-PFS_{53} were prepared according to previously reported methods (Figure 1).[29] Transmission electron microscopy (TEM) (Figures 2, S1, and S2)

Table 1. Polymer Characterization Data

polymer	M_n first block ($g\ mol^{-1}$)[a]	block ratio[b]	M_n diblock ($g\ mol^{-1}$)[b]	PDI[a]
PFS_{28}-*b*-$PDMS_{560}$ (**2**)	6 700	1:20	48 200	1.02
PI_{637}-*b*-PFS_{53} (**3**)	43 400	12:1	56 300	1.01

[a] Determined by triple detection GPC analysis. [b] Determined by relative integration of ^{1}H NMR signals from each block.

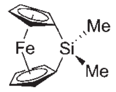

1

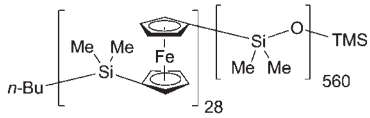

2: PFS_{28}-*b*-$PDMS_{560}$

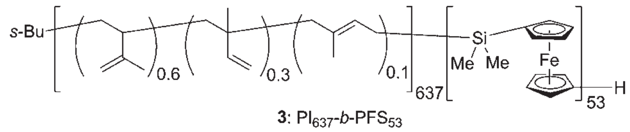

3: PI_{637}-*b*-PFS_{53}

was used to determine the length distribution of the PI_{637}-*b*-PFS_{53} cylindrical micelles (core radius ~7.0 nm, L_n = 1160 nm, L_w = 1210 nm, L_w/L_n = 1.04, σ/L_n = 0.20), which were grown from small PFS_{28}-*b*-$PDMS_{560}$ crystallites (L_n = 23 nm, L_w = 24 nm, L_w/L_n = 1.04, σ/L_n = 0.13) obtained via sonication of long (>5 μm) cylindrical micelles (Figures S3 and S4) by manually tracing the electron-rich cores of 500 individual micelles. The height (~10 nm) and overall width (~50 nm) of the micelles were determined by examination of atomic force microscopy (AFM) height images (Figures 2 and S5), where both the micelle core and corona contribute to the measurements.[36]

The liquid-crystalline properties of rigid rods in solution have been of interest since the development of Onsager theory in the 1940s.[37] The theory describes the liquid-crystalline behavior of hard rigid rods as a function of aspect ratio and concentration. As the aspect ratio of rigid rods increases, the relative concentration required to access liquid-crystalline phases (e.g., nematic and smectic) decreases. The theory has been revisited several times,[38] primarily due to advances in modern computing power, and variables such as the polydispersity of the rigid rods have been explored.[39] Many examples of liquid crystals based on suspensions of surfactant-stabilized inorganic rigid rods have been described in the literature;[40] however, fewer examples based on self-assembled block copolymers (i.e., soft matter) have been described,[19] perhaps due to the potential for concentration-dependent morphology changes. In this study we utilized the I22 small-angle X-ray scattering instrument at the Diamond Synchrotron operating at a wavelength of 1.0 Å and a detector distance of 6.0 m for SAXS studies which were used to confirm the dimensions and orientational order of the micelles in a field-responsive nematic-like liquid-crystalline phase (Figure S6). A wavelength of 0.62 Å and a detector distance of 0.6 m were used for WAXS studies. The high intensity of the X-ray source combined with the short wavelength and short detector distance were required to probe the internal structure of the micelle core.

The SAXS from solutions of perfectly rigid rods is expected to be highly anisotropic if their long axes are aligned in a given

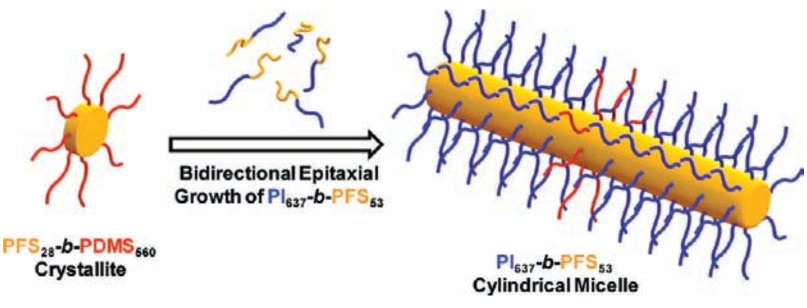

Figure 1. Formation of monodisperse PI_{637}-*b*-PFS_{53} cylindrical micelles via bidirectional epitaxial growth from small, uniform, stub-like PFS_{28}-*b*-$PDMS_{560}$ crystallites. The polymers used in this study are shown in orange (PFS), red (PDMS), and blue (PI).

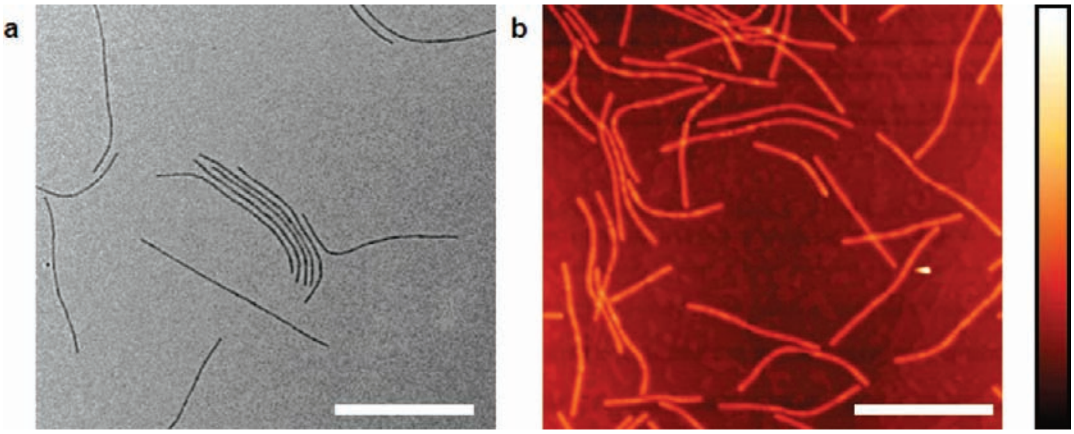

Figure 2. (a) Bright-field TEM image of 1160 nm PI_{637}-*b*-PFS_{53} cylindrical micelles drop-cast onto a carbon-coated copper grid. (b) AFM height image of PI_{637}-*b*-PFS_{53} cylindrical micelles drop-cast onto highly ordered pyrolytic graphite. Horizontal scale bars correspond to 1000 nm, and the vertical scale bar in (b) corresponds to 0−40 nm. The RMS background of the AFM height image is 0.54 nm.

direction. If the alignment is perfect, the extent of the scattering is inversely proportional to the dimension of the particle; therefore, the scattering parallel to the preferred direction would be confined to a scattering vector, $Q_{\parallel}$, less than $\sim 10^{-3}$ Å^{-1}, but that perpendicular to the preferred direction would extend to scattering vector $Q_{\perp} \approx 10^{-1}$ Å^{-1}. Thus, rods aligned horizontally would give a narrow, vertical streak in the diffraction pattern. If the alignment is not perfect, the streak broadens, and the distribution of the scattered intensity around a ring of constant Q can be used to determine the orientational order parameter, S, of the rods (see Supporting Information for details). The order parameter would have a value of 1 for perfect alignment of the long axes of the rods parallel to the applied electric field, zero for random alignment, and −0.5 for alignment perpendicular to the field.

A 75 mg mL^{-1} solution of 1160 nm long PI_{637}-*b*-PFS_{53} cylindrical micelles in decane was studied by SAXS in the presence of an alternating current (1 kHz) electric field of 4.0 V μm^{-1} (peak to peak).[41] In the presence of an electric field, the long axis of the cylindrical micelles aligned in the direction of the applied field (Figures 3a and S7). Using the distribution of intensity in rings of radius 0.14−0.36 Å^{-1}, the order parameter was determined to be $S \approx 0.77$.[42] This value is comparable to those observed for the previously studied 50 mg mL^{-1} decane solution of 730 nm PI_{550}-*b*-PFS_{50} cylindrical micelles in a similar electric field ($S = 0.73$)[29] and solutions of the relatively lower aspect ratio tobacco mosaic virus in a magnetic field ($S = 0.77$).[43]

A vertical section from the data in Figure 3a is shown in Figure 4. At low $Q_{\perp}$, there are some inter-rod interference peaks which arise from translational ordering of the rod axes. This feature will be discussed in detail in a future publication. At higher $Q_{\perp}$, the inter-rod interference appears to have decayed, and so the intensity can be analyzed using a model for the scattering from a rigid cylindrical rod,

$$I(Q_{\perp}) \propto \frac{1}{Q_{\perp}}\left(\frac{2J_1(Q_{\perp}R)}{Q_{\perp}R}\right)^2 \qquad (1)$$

where J_1 is a cylindrical Bessel function and R is the radius of the rod.[44,45] Polydispersity of the radius may be accounted for by averaging over a distribution of R values. The fit shown in Figure 4 corresponds to a mean radius of 4.7 nm and a Gaussian distribution of radii with standard deviation 1.0 nm. This was interpreted as the core radius because the diffuse polyisoprene corona is expected to have electron density similar to that of the decane solvent and significantly less than that of the PFS core.

As noted above, the mechanism of seeded growth upon introduction of additional PFS or polyferrocenyldimethylgermane (PFG) diblock copolymers in solution is believed to involve epitaxy from the ends of the crystalline PFS core of cylindrical micelles.[32] We therefore also acquired WAXS data for the same field-aligned sample of cylindrical micelles in decane in order to gain insight into the structure of the crystalline core derived from the PFS block that is formed during solution self-assembly. The diffraction shown in Figure 3b has had background from pure solvent subtracted. The uniaxial alignment of the sample means that the long axes of the micelles tend to be parallel to the applied field. The short axes tend to be perpendicular to the field but are distributed uniformly about the field. Thus, the WAXS results in Figure 3b represent an average of all orientations of the micelles about the field (Figure S9). The 2D diffraction pattern contains six Bragg peaks at 60° intervals around a circle, with two of the Bragg peaks occurring at slightly different values of Q. We therefore infer that the diffraction pattern, which is consistent with the pattern previously obtained during electron diffraction studies of platelet micelles formed by PFS-containing block copolymers of different composition, arises from a crystalline phase with pseudo-hexagonal symmetry (i.e., it does not possess perfect *d*6 symmetry).[32] Since the orientational order of the rods with respect to the field is high ($S = 0.77$), and assuming that there is no preferred orientation perpendicular to the field, this pattern indicates that, in every micelle, the hexagonal axis is perpendicular to the rod axis. On the basis of this alone, it is not possible to conclude whether the micelle cores are single-crystalline domains or whether there are several different domains present in a rod with hexagonal axes distributed about the rod axis. However, the full width at half-maximum of the peaks in the transverse direction is about 15°, which indicates a very high orientational order parameter (∼0.9). This is consistent with the interior of the micelles being a crystalline monodomain and also suggests that the order parameters from the SAXS may be underestimated.

The radial distributions of the peaks were analyzed in detail by taking a 15° wide sector centered on each peak and regrouping the intensity as intensity vs Q. These data were then fitted with a Gaussian peak shape on a linear background (Figure 5). It was

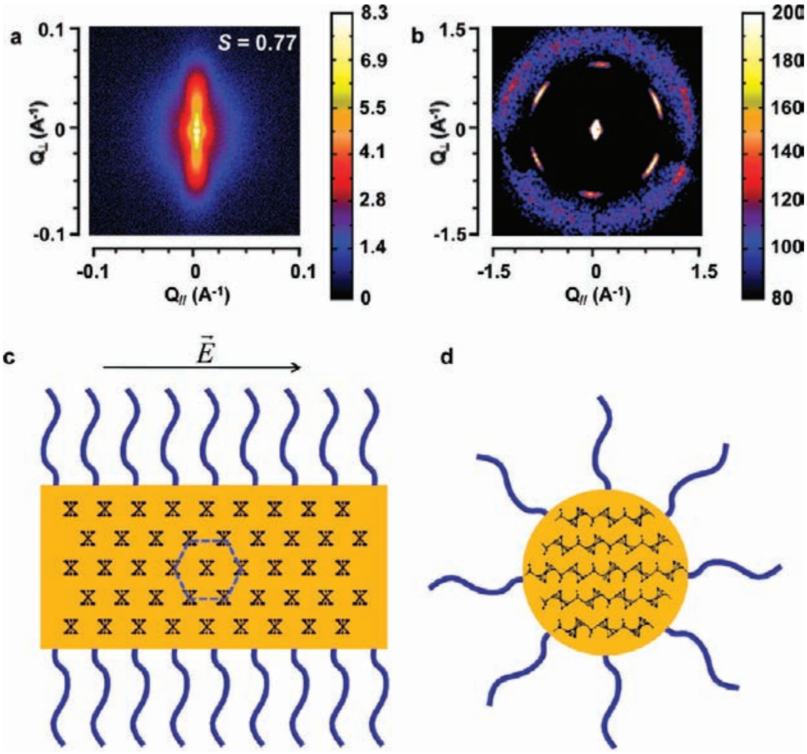

Figure 3. (a) SAXS and (b) WAXS patterns for a 75 mg mL^{-1} decane solution of 1160 nm long PI_{637}-*b*-PFS_{53} cylindrical micelles in a 4.0 V μm^{-1} electric field. The pseudo-hexagonal pattern shown in (b) is offset by 3° due to a small misalignment of the applied electric field. Idealized representations (not to scale) of (c) side view and (d) end view of a crystalline PFS cylindrical micelle core. The incident X-rays were perpendicular to the applied electric field and to the plane of (c). The PFS chains are packed in a 2D lattice with pseudo-hexagonal symmetry, perpendicular to the long axis of the cylindrical micelle. The micelle core may also possess a disordered or amorphous region near the core−corona/solvent interface. The vertical scale bars in (a) and (b) represent log(intensity) of the scattered X-rays.

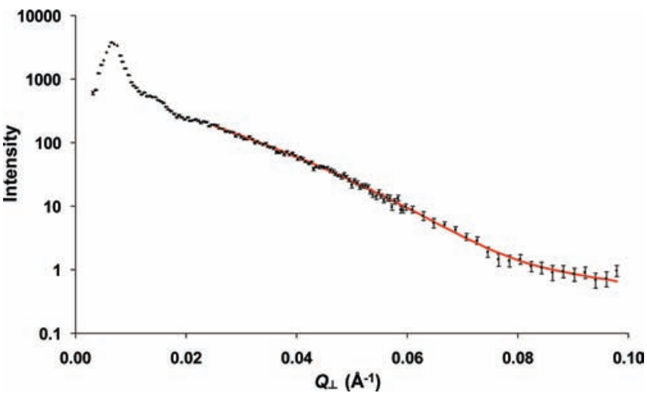

Figure 4. Plot of intensity vs $Q_\perp$ from the SAXS results for the 75 mg mL^{-1} solution of 1160 nm long PI_{637}-*b*-PFS_{53} cylindrical micelles in a 4.0 V μm^{-1} electric field. The line is a fit of the model described in the text.

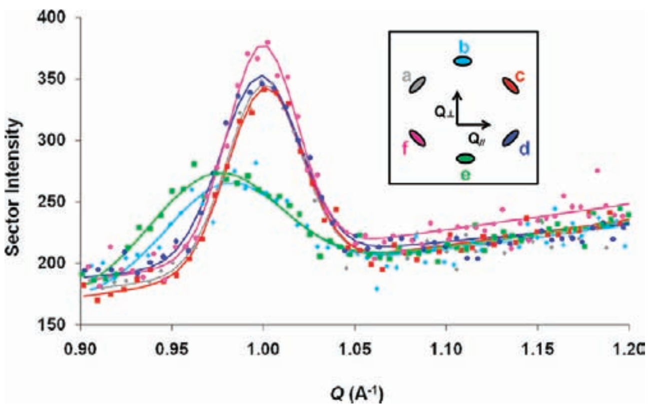

Figure 5. Plots showing Gaussian fits to the radial sections across each of the peaks observed in the WAXS pattern obtained for a sample of 1160 nm long PI_{637}-*b*-PFS_{53} cylindrical micelles in decane in a 4.0 V μm^{-1} electric field. The inset represents the scattering observed in Figure 3b.

found that two peaks (labeled b and e) were at slightly lower Q (0.977 Å^{-1}) than the other four (labeled a, c, d, and f, Q = 1.000 Å^{-1}) and were also broader (Figure 5). Thus, there are crystal planes (corresponding to peaks b and e) spaced by 6.43 Å lying parallel to the rod axis and planes spaced by 6.29 Å tilted with respect to the rod axes.[46] The widths of the peaks may arise from particle size broadening effects. For a Bragg peak at a scattering vector exactly perpendicular to a cylindrical rod, a Guinier approximation can be used to show that the standard deviation (σ) of the radial peak profile is related to the rod radius, R, by[45,47]

$$R = \frac{\sqrt{2}}{\sigma} \tag{2}$$

The fits to peaks b and e give σ = 0.35 nm^{-1}, giving R = 4.1 ± 0.3 nm. This value is in excellent agreement with the radius

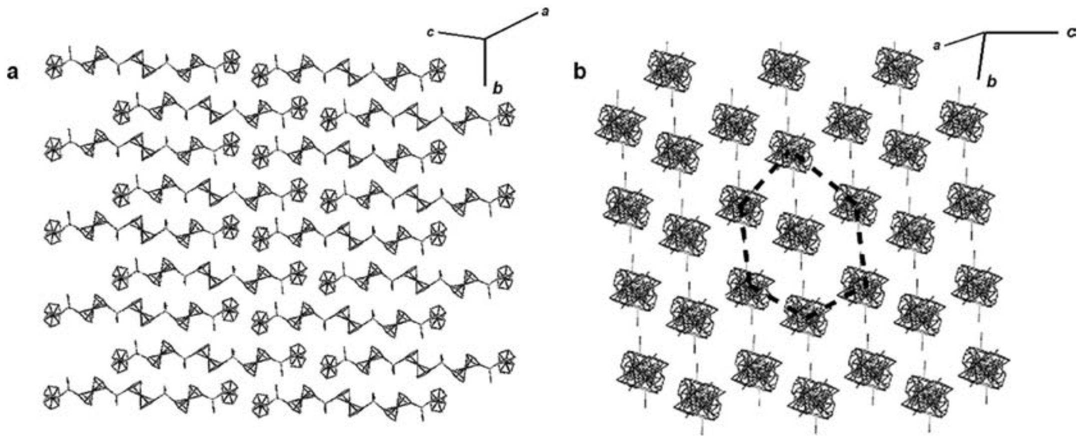

Figure 6. Pseudo-hexagonal packing viewed (a) perpendicular and (b) parallel to the linear pentamer chains in the crystal lattice of **4**.[54]

determined from the SAXS data. The fits to peaks a, c, d, and f give $\sigma = 0.20\ \mathrm{nm}^{-1}$, giving $R = 7.0 \pm 0.3$ nm. This is consistent with the factor of 2 which arises because the planes' normal is at 30° to the rod axis rather than perpendicular to it (see Supporting Information for more details). The agreement between the radii determined from the two different sources indicates that there are no sources of peak broadening other than the cutoff of the crystal structure at the rod radius. This provides a further indication that the crystalline domains within the micelle core are highly ordered. The radii of the crystalline PFS domains within the micelle core are significantly lower than obtained by TEM analysis, ~7.0 nm, which allows for direct observation of the electron-rich micelle core. This may be an indication that the outer, curved portion of the micelle core is in fact comprised of a disordered, amorphous region of PFS chains. This hypothesis is consistent with the assumption that chain folding must occur within the micelle core, and that regions of the core that are rich in chain folds are not expected to be crystalline.[48] Another possible interpretation for the difference between the radii determined by TEM and X-ray scattering studies is that the micelle cores are anisotropic (i.e., elliptical) in terms of their cross-section.[49] The PFS chains are packed pseudo-hexagonally along the major axis; therefore, the line-broadening studies from the WAXS data give an average radius for the minor axis of 4.1 ± 0.3 nm. The TEM studies yield a radius of ~7 nm, which may be more sensitive to the dimensions of the major axis, but may also be influenced by interactions between the micelle and the hydrophobic substrate employed. The SAXS data yield an intermediate value (4.7 ± 1.0 nm), as there is no preferred micelle orientation perpendicular to the applied electric field, which is consistent with this interpretation. Previous studies of cross-sectioned shell-cross-linked cylinders of PI-*b*-PFS were consistent with a curved core cross-section rather than a flat ribbon structure.[22] However, the data would not be expected to distinguish between circular and elliptical cross-sections.

■ DISCUSSION

There have been several reports on the crystallization and crystal structure of PFS homopolymers, with varying results depending on sample preparation.[50−55] High-molecular-weight samples of PFS drop-cast from benzene solutions showed an intense maximum *d*-spacing of 6.34 Å when studied by WAXS,[51] while melt-crystallized samples of PFS showed two sharp reflections at 6.02 and 6.65 Å.[52] Finally, extrusion methods have been used to study oriented PFS fibers. For these samples a maximum *d*-spacing of 6.36 Å along the equator of the extruded fiber was reported, and this led to the conclusion that PFS crystallized in the monoclinic crystalline phase ($a = 13.29$ Å, $b = 6.01$ Å, $c = 13.9$ Å, and $\gamma = 93.6°$).[53]

For our purposes, a particularly useful study for interpretation of the present results involves the packing within the crystal structure of the linear pentamer of ferrocenyldimethylsilane **4**, which takes place in a pseudo-hexagonal fashion (Figure 6).[54] The strongest reflection in the powder pattern of **4**, corresponding to a *d*-spacing of 6.287 Å, has previously been assigned to planes with [0 1 1] Miller indices.[55] This distance corresponds well with the strongest reflections observed in the WAXS studies of PFS homopolymers and provides significant evidence that the most intense reflections observed for the crystalline micelle cores correspond to Miller planes approximately parallel to the polymer chains with *d*-spacings corresponding to the interchain packing distances.

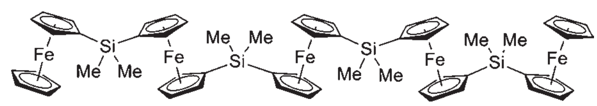

4

Further inspection of the powder pattern of **4** reveals that the next two most intense reflections also correspond to planes with [1 −2 0] (d = 5.904 Å) and [1 −1 1] (d = 6.580 Å) Miller indices, each approximately parallel to the pentamer chains in the crystal structure.[55] The WAXS scattering observed for the cylindrical micelles is similar to that observed for the linear pentamer; however, the structure of the micelle core has relatively higher symmetry with two closely related *d*-spacings (6.29 and 6.43 Å), which can be assigned to interchain packing distances. Using the single-crystal X-ray structure of the linear pentamer of ferrocenyldimethylsilane **4** as a model, we can approximate the intramolecular Fe−Fe distances in the crystalline PFS micelle core as 6.056(5) and 6.913(5) Å. Based on the number-average degree of polymerization of the PFS block in PI_{637}-*b*-PFS_{53} (determined by GPC) and the average intramolecular Fe−Fe distance, the estimated contour length of the PFS block is ~34 nm. Comparison of the contour length and the cylinder dimensions determined from the SAXS studies allows for the conclusion that each of the PFS chains folds on average at least four times in the crystalline micelle core. Furthermore, on the basis of the average *d*-spacing, we estimate that up to 15 folded polymer segments may pack together in order to span the diameter of the crystalline core.

SUMMARY

We have studied the crystal structure of the PFS core of cylindrical micelles based on PFS-containing block copolymers. By taking advantage of the field-responsive behavior of monodisperse PI_{637}-*b*-PFS_{53} cylindrical micelles, we were able to determine that the PFS chains pack in a lattice with 2D pseudohexagonal symmetry perpendicular to the long axis of the micelle core with *d*-spacings of 6.29 and 6.43 Å. With the knowledge of the micelle core structure gained in this study, we are now able to suggest a mechanism for the interesting crystalline-driven living self-assembly process established for these PFS metalloblock copolymer systems.[29,30,32] The epitaxial growth appears to involve efficient packing (perpendicular to the cylinder long axis) of the PFS segment of the added block copolymer at the ends of crystalline PFS domains, resulting in a controlled increase in cylinder length. A similar mechanism may operate with PFS platelet micelles, which exhibit analogous epitaxial growth phenomena predominantly along the direction of their long axis,[32] and cylinders formed by all-organic systems, which display similar self-assembly behavior.[20] Future work will aim to place these assertions for micelles based on other crystalline-core block copolymers on a firm experimental basis. Of particular interest in this regard are micelles based on π-conjugated structures, which are expected to possess interesting and potentially useful electronic and optical properties.[20b,27h]

ASSOCIATED CONTENT

S Supporting Information. Experimental details, detailed SAXS and WAXS data treatment, additional microscopy figures, histograms, and 1D WAXS data. This material is available free of charge via the Internet at http://pubs.acs.org.

AUTHOR INFORMATION

Corresponding Author
mwinnik@chem.utoronto.ca; ian.manners@bristol.ac.uk; robert.richardson@bristol.ac.uk

ACKNOWLEDGMENT

The authors gratefully acknowledge the Diamond Lightsource Synchrotron facility for a beamtime award (SM6035) and the European Union (EU) for financial support of this work. J.B.G. and P.A.R. are grateful to the NSERC of Canada and to the EU for postdoctoral fellowships. I.M. thanks the EU for a Marie Curie Chair and a Reintegration Grant, the European Research Council for an Advanced Investigator Grant, and the Royal Society for a Wolfson Research Merit Award. M.A.W. thanks the NSERC of Canada for financial support. The authors also thank Dr. Torben Gädt for synthesizing PFS_{28}-*b*-$PDMS_{560}$, Dr. John M. Mitchels for assistance with AFM experiments, and Mr. Alexander J. Robertson for his role in analyzing SAXS data.

REFERENCES

(1) (a) Mao, C.; Solis, D. J.; Reiss, B. D.; Kottmann, S. T.; Sweeney, R. Y.; Hayhurst, A.; Georgiou, G.; Iverson, B.; Belcher, A. M. *Science* **2004**, *303*, 213–217. (b) Nam, K. T.; Kim, D.-W.; Yoo, P. J.; Chiang, C.-Y.; Meethong, N.; Hammond, P. T.; Chiang, Y.-M.; Belcher, A. M. *Science* **2006**, *312*, 885–888. (c) Tseng, R. J.; Tsai, C.; Ma, L.; Ouyang, J.; Ozkan, C. S.; Yang, Y. *Nat. Nanotechnol.* **2006**, *1*, 72–77. (d) Tian, B.; Zheng, X.; Kempa, T. J.; Fang, Y.; Yu, N.; Yu, G.; Huang, J.; Lieber, C. M. *Nature* **2007**, *449*, 885–890.

(2) (a) Palmer, L. C.; Stupp, S. I. *Acc. Chem. Res.* **2008**, *41*, 1674–1684. (b) Zhao, Y. S.; Fu, H.; Peng, A.; Ma, Y.; Liao, Q.; Yao, J. *Acc. Chem. Res.* **2010**, *43*, 409–418.

(3) Mann, S. *Nat. Mater.* **2009**, *8*, 781–792.

(4) Nie, Z.; Petukhova, A.; Kumacheva, E. *Nat. Nanotechnol.* **2010**, *5*, 15–25.

(5) Douglas, T.; Young, M. *Science* **2006**, *312*, 873–875.

(6) (a) Xia, Y.; Yang, P.; Sun, Y.; Wu, Y.; Mayers, B.; Gates, B.; Yin, Y.; Kim, F.; Yan, H. *Adv. Mater.* **2003**, *15*, 353–389. (b) Cademartiri, L.; Ozin, G. A. *Adv. Mater.* **2009**, *21*, 1013–1020.

(7) (a) de Heer, W. A. *Nat. Mater.* **2002**, *1*, 153–154. (b) Baughman, R. H.; Zakhidov, A. A.; de Heer, W. A. *Science* **2002**, *297*, 787–792.

(8) (a) Sheiko, S. S.; Sumerlin, B. S.; Matyjaszewski, K. *Prog. Polym. Sci.* **2008**, *33*, 759–785. (b) Feng, C.; Li, Y.; Yang, D.; Hu, J.; Zhang, X.; Huang, X. *Chem. Soc. Rev.* **2011**, *40*, 1282–1295.

(9) Wegner, G. *Macromol. Chem. Phys.* **2003**, *204*, 347–357.

(10) Smith, A. M.; Acquah, S. F. A.; Bone, N.; Kroto, H. W.; Ryadnov, M. G.; Stevens, M. S. P.; Walton, D. R. M.; Woolfson, D. N. *Angew. Chem., Int. Ed.* **2005**, *44*, 325–328.

(11) (a) Cameron, N. S.; Corbierre, M. K.; Eisenberg, A. *Can. J. Chem.* **1999**, *77*, 1311–1326. (b) Zhulina, E. B.; Adam, M.; LaRue, I.; Sheiko, S. S.; Rubinstein, M. *Macromolecules* **2005**, *38*, 5330–5351. (c) Hayward, R. C.; Pochan, D. J. *Macromolecules* **2010**, *43*, 3577–3584.

(12) (a) Li, Z.; Chen, Z.; Cui, H.; Hales, K.; Qi, K.; Wooley, K. L.; Pochan, D. J. *Langmuir* **2005**, *21*, 7533–7539. (b) Schleuss, T. W.; Abbel, R.; Gross, M.; Schollmeyer, D.; Frey, H.; Maskos, M.; Berger, R.; Kilbinger, A. F. M. *Angew. Chem., Int. Ed.* **2006**, *45*, 2969–2975.

(13) (a) Cornelissen, J. J. L. M.; Fischer, M.; Sommerdijk, N. A. J. M.; Nolte, R. J. M. *Science* **1998**, *280*, 1427–1430. (b) Dupont, J.; Liu, G.; Niihara, K.-i.; Kimoto, R.; Jinnai, H. *Angew. Chem., Int. Ed.* **2009**, *48*, 6144–6147.

(14) Pochan, D. J.; Chen, Z.; Cui, H.; Hales, K.; Qi, K.; Wooley, K. L. *Science* **2004**, *306*, 94–97.

(15) Discher, D. E.; Eisenberg, A. *Science* **2002**, *297*, 967–973.

(16) (a) Yu, K.; Zhang, L.; Eisenberg, A. *Langmuir* **1996**, *12*, 5980–5984. (b) Zhang, L.; Bartels, C.; Yu, Y.; Shen, H.; Eisenberg, A. *Phys. Rev. Lett.* **1997**, *79*, 5034–5037. (c) Stewart, S.; Liu, G. *Angew. Chem., Int. Ed.* **2000**, *39*, 340–344. (d) Li, Z.; Kesselman, E.; Talmon, Y.; Hillmyer, M. A.; Lodge, T. P. *Science* **2004**, *306*, 98–101. (e) Kubowicz, S.; Baussard, J.-F.; Lutz, J.-F.; Thünemann, A. F.; von Berlepsch, H.; Laschewsky, A. *Angew. Chem., Int. Ed.* **2005**, *44*, 5262–5265. (f) Voets, I. K.; de Keizer, A.; de Waard, P.; Frederik, P. M.; Bomans, P. H. H.; Schmalz, H.; Walther, A.; King, S. M.; Leermakers, F. A. M.; Cohen Stuart, M. A. *Angew. Chem., Int. Ed.* **2006**, *45*, 6673–6676. (g) Walther, A.; André, X.; Drechsler, M.; Abetz, V.; Müller, A. H. E. *J. Am. Chem. Soc.* **2007**, *129*, 6187–6198. (h) Saito, N.; Liu, C.; Lodge, T. P.; Hillmyer, M. A. *Macromolecules* **2008**, *41*, 8815–8822. (i) Walther, A.; Drechsler, M.; Rosenfeldt, S.; Harnau, L.; Ballauff, M.; Abetz, V.; Müller, A. H. E. *J. Am. Chem. Soc.* **2009**, *131*, 4720–4728.

(17) Qian, J.; Zhang, M.; Manners, I.; Winnik, M. A. *Trends Biotechnol.* **2010**, *28*, 84–92.

(18) (a) Zhang, L.; Eisenberg, A. *Science* **1995**, *268*, 1728–1731. (b) Spatz, J. P.; Mössmer, S.; Möller, M. *Angew. Chem., Int. Ed.* **1996**, *35*, 1510–1512. (c) Liu, G.; Ding, J.; Qiao, L.; Guo, A.; Dymov, B. P.; Gleeson, J. T.; Hashimoto, T.; Saijo, K. *Chem.—Eur. J.* **1999**, *5*, 2740–2749. (d) Jain, S.; Bates, F. S. *Science* **2003**, *300*, 460–464. (e) Jain, S.; Bates, F. S. *Macromolecules* **2004**, *37*, 1511–1523. (f) Korczagin, I.; Hempenius, M. A.; Fokkink, R. G.; Cohen Stuart, M. A.; Al-Hussein, M.; Bomans, P. H. H.; Frederik, P. M.; Vancso, G. J. *Macromolecules* **2006**, *39*, 2306–2315. (g) Wurm, F.; Hilf, S.; Frey, H. *Chem.—Eur. J.* **2009**, *15*, 9068–9077.

(19) Won, Y.-Y.; Davis, H. T.; Bates, F. S. *Science* **1999**, *283*, 960–963.

(20) (a) Petzetakis, N.; Dove, A. P.; O'Reilly, R. K. *Chem. Sci.* **2011**, *2*, 955–960. (b) Patra, S. K.; Ahmed, R.; Whittell, G. R.; Lunn, D. J.;

Dunphy, E. L.; Winnik, M. A.; Manners, I. *J. Am. Chem. Soc.* **2011**, *133*, 8842–8845.

(21) (a) Yan, X.; Liu, G.; Haeussler, M.; Tang, B. Z. *Chem. Mater.* **2005**, *17*, 6053–6059. (b) Wang, H.; Lin, W.; Fritz, K. P.; Scholes, G. D.; Winnik, M. A.; Manners, I. *J. Am. Chem. Soc.* **2007**, *129*, 12924–12925. (c) Wang, H.; Wang, X.; Winnik, M. A.; Manners, I. *J. Am. Chem. Soc.* **2008**, *130*, 12921–12930.

(22) Wang, X.; Liu, K.; Arsenault, A. C.; Rider, D. A.; Ozin, G. A.; Winnik, M. A.; Manners, I. *J. Am. Chem. Soc.* **2007**, *129*, 5630–5639.

(23) Dean, J. M.; Verghese, N. E.; Pham, H. Q.; Bates, F. S. *Macromolecules* **2003**, *36*, 9267–9270.

(24) Cao, L.; Massey, J. A.; Winnik, M. A.; Manners, I.; Riethmüller, S.; Banhart, F.; Spatz, J. P.; Möller, M. *Adv. Funct. Mater.* **2003**, *13*, 271–276.

(25) (a) Dalhaimer, P.; Engler, A. J.; Parthasarathy, R.; Discher, D. E. *Biomacromolecules* **2004**, *5*, 1714–1719. (b) Geng, Y.; Dalhaimer, P.; Cai, S.; Tsai, R.; Tewari, M.; Minko, T.; Discher, D. E. *Nat. Nanotechnol.* **2007**, *2*, 249–255.

(26) (a) Thurmond, K. B., II; Kowalewski, T.; Wooley, K. L. *J. Am. Chem. Soc.* **1996**, *118*, 7239–7240. (b) Tao, J.; Liu, G.; Ding, J.; Yang, M. *Macromolecules* **1997**, *30*, 4084–4089. (c) Ding, J.; Liu, G. *Macromolecules* **1998**, *31*, 6554–6558. (d) O'Reilly, R. K.; Hawker, C. J.; Wooley, K. L. *Chem. Soc. Rev.* **2006**, *35*, 1068–1083. (e) Read, E. S.; Armes, S. P. *Chem. Commun.* **2007**, 3021–3035. (f) van Nostrum, C. F. *Soft Matter* **2011**, *7*, 3246–3259.

(27) (a) Fu, J.; Luan, B.; Yu, X.; Cong, Y.; Li, J.; Pan, C.; Han, Y.; Yang, Y.; Li, B. *Macromolecules* **2004**, *37*, 976–986. (b) Zhang, J.; Wang, L.-Q.; Wang, H.; Tu, K. *Biomacromolecules* **2006**, *7*, 2492–2500. (c) Du, Z.-X.; Xu, J.-T.; Fan, Z.-Q. *Macromolecules* **2007**, *40*, 7633–7637. (d) Portinha, D.; Boué, F.; Bouteiller, L.; Carrot, G.; Chassenieux, C.; Pensec, S.; Reiter, G. *Macromolecules* **2007**, *40*, 4037–4042. (e) Lazzari, M.; Scalarone, D.; Vazquez-Vazquez, C.; López-Quintela, M. A. *Macromol. Rapid Commun.* **2008**, *29*, 352–357. (f) Schmalz, H.; Schmelz, J.; Drechsler, M.; Yuan, J.; Walther, A.; Schweimer, K.; Mihut, A. M. *Macromolecules* **2008**, *41*, 3235–3242. (g) Mihut, A. M.; Drechsler, M.; Möller, M.; Ballauff, M. *Macromol. Rapid Commun.* **2010**, *31*, 449–453. (h) Lee, E.; Hammer, B.; Kim, J.-K.; Page, Z.; Emrick, T.; Hayward, R. C. *J. Am. Chem. Soc.* **2011**, *133*, 10390–10393.

(28) The crystallinity of the micelle cores may also be advantageous in solution-based studies due to their kinetically frozen nature, which precludes concentration-dependent morphology changes.

(29) Gilroy, J. B.; Gädt, T.; Whittell, G. R.; Chabanne, L.; Mitchels, J. M.; Richardson, R. M.; Winnik, M. A.; Manners, I. *Nat. Chem.* **2010**, *2*, 566–570.

(30) Wang, X.; Guerin, G.; Wang, H.; Wang, Y.; Manners, I.; Winnik, M. A. *Science* **2007**, *317*, 644–647.

(31) Feng, H.; Gädt, T.; Manners, I.; Winnik, M. A. *J. Am. Chem. Soc.* **2011**, *133*, 9095–9103.

(32) Gädt, T.; Ieong, N. S.; Cambridge, G.; Winnik, M. A.; Manners, I. *Nat. Mater.* **2009**, *8*, 144–150.

(33) Soto, A. P.; Gilroy, J. B.; Winnik, M. A.; Manners, I. *Angew. Chem., Int. Ed.* **2010**, *49*, 8220–8223.

(34) Gädt, T.; Schacher, F. S.; McGrath, N.; Winnik, M. A.; Manners, I. *Macromolecules* **2011**, *44*, 3777–3786.

(35) (a) Ni, Y.; Rulkens, R.; Manners, I. *J. Am. Chem. Soc.* **1996**, *118*, 4102–4114. (b) Massey, J. A.; Temple, K.; Cao, L.; Rharbi, Y.; Raez, J.; Winnik, M. A.; Manners, I. *J. Am. Chem. Soc.* **2000**, *122*, 11577–11584.

(36) The asymmetry of the cylindrical micelles as measured by AFM implies significant interaction of the corona-forming polyisoprene block with the HOPG substrate, causing the micelle to "spread" over the substrate.

(37) Onsager, L. *Ann. N.Y. Acad. Sci.* **1949**, *51*, 627–659.

(38) (a) McGrother, S. C.; Williamson, D. C.; Jackson, G. *J. Chem. Phys.* **1996**, *104*, 6755–6771. (b) Bolhuis, P.; Frenkel, D. *J. Chem. Phys.* **1997**, *106*, 666–687.

(39) Bates, M. A.; Frenkel, D. *J. Chem. Phys.* **1998**, *109*, 6193–6199.

(40) (a) Vroege, G. J.; Thies-Weesie, D. M. E.; Petukhov, A. V.; Lemaire, B. J.; Davidson, P. *Adv. Mater.* **2006**, *18*, 2565–2568. (b) Meuer, S.; Oberle, P.; Theato, P.; Tremel, W.; Zentel, R. *Adv. Mater.* **2007**, *19*, 2073–2078. (c) Dessombz, A.; Chiche, D.; Davidson, P.; Panine, P.; Chanéac, C.; Jolivet, J.-P. *J. Am. Chem. Soc.* **2007**, *129*, 5904–5909.

(41) The sample of 1160 nm PI_{637}-*b*-PFS_{53} cylindrical micelles was studied after the X-ray scattering studies, confirming that the samples had not changed signficantly (L_n = 1210 nm, L_w =1310 nm, L_w/L_n = 1.08, σ/L_n = 0.28). The slightly broadened length distribution may be due to mechanical stress induced during sample preparation, manipulation with an electric field, or sample extraction. See Figure S1 for details.

(42) The calculated order parameter (S) remained relatively constant over a Q range of 0.007−0.044 $Å^{-1}$. See Figure S8 for details.

(43) Oldenbourg, R.; Wen, X.; Meyer, R. B.; Caspar, D. L. D. *Phys. Rev. Lett.* **1988**, *61*, 1851–1854.

(44) Fournet, G. *Bull. Soc. Fr. Mineral Cryst.* **1951**, *74*, 39–113.

(45) Guinier, A.; Fournet, G. *Small angle scattering of X-rays*; John Wiley & Sons Inc.: New York, 1955.

(46) The *d*-spacings associated with the micelle core structure were consistent with the most intense reflection obtained during 1D WAXS studies of a film of cylindrical micelles drop-cast onto a silicon substrate. See Figure S10 for details.

(47) Guinier, A. *Ann. Phys.* **1939**, *12*, 161–237.

(48) Ungar, G.; Zeng, X.-b. *Chem. Rev.* **2001**, *101*, 4157–4188.

(49) It should be noted that it is notoriously difficult to distinguish between polydisperse rods and elliptical structures using the models employed in this study.

(50) Xu, J.; Ma, Y.; Hu, W.; Rehahn, M.; Reiter, G. *Nat. Mater.* **2009**, *8*, 348–353.

(51) Nguyen, M. T.; Diaz, A. F.; Dement'ev, V. V.; Pannell, K. H. *Chem. Mater.* **1993**, *5*, 1389–1394.

(52) Lammertink, R. G. H.; Hempenius, M. A.; Manners, I.; Vancso, G. J. *Macromolecules* **1998**, *31*, 795–800.

(53) Papkov, V. S.; Gerasimov, M. V.; Dubovik, I. I.; Sharma, S.; Dementiev, V. V.; Pannell, K. H. *Macromolecules* **2000**, *33*, 7107–7115.

(54) Rulkens, R.; Lough, A. J.; Manners, I.; Lovelace, S. R.; Grant, C.; Geiger, W. E. *J. Am. Chem. Soc.* **1996**, *118*, 12683–12695.

(55) Rasburn, J.; Petersen, R.; Jahr, T.; Rulkens, R.; Manners, I.; Vancso, G. J. *Chem. Mater.* **1995**, *7*, 871–877.